https://doi.org/10.37434/tpwj2020.01.02

NUMERICAL PREDICTION OF THE STATE OF BEAM PRODUCTS OF DIFFERENT THICKNESS DURING LAYER-BY-LAYER ELECTRON BEAM SURFACING

O.S. Milenin[1], **O.A. Velikoivanenko**[1], **S.S. Kozlitina**[1], **S.M. Kandala**[1] and **A.E. Babenko**[2]
[1]E.O. Paton Electric Welding Institute of the NAS of Ukraine
11 Kazymyr Malevych Str., 03150, Kyiv, Ukraine. E-mail: office@paton.kiev.ua
[2]National Technical University of Ukraine «Igor Sikorsky Kyiv Polytechnic Institute»
37 Peremohy Prosp., 03056. Kyiv, Ukraine

A complex of mathematical models and their computer realization means for numerical prediction of the kinetics of temperature fields, phase and structural states, mechanical stresses and strains in layer-by-layer formation of typical products of titanium-based alloys was developed. The peculiarities of VT6 titanium alloy state kinetics, depending on the technological parameters of production, were investigated on the typical examples of electron beam surfacing of T-shaped beam structures, from these alloys produced by xBeam 3D Metal Printer technology. The impact of the substrate thickness on the regularities of temperature field development during layer-by-layer formation of beam elements and on the structural state of the metal after complete cooling is shown. In the case of forming a thick-walled T-shaped product, it is shown that an important factor that allows obtaining a low level of residual stresses, is optimization of the delay time between deposition of each of the beads, to provide the conditions for uniform cooling of the structure. 11 Ref., 14 Figures.

Keywords: additive technologies, electron beam surfacing, xbeam 3D Metal Printer, mathematical modeling, macrostructure, mechanical properties, stress-strain state

Broad introduction of additive technologies is a sustainable modern trend, when designing production schemes of critical structural elements of a complex shape. In particular, the schemes of electron beam surfacing (EBS) of parts from light metals (primarily, titanium and aluminium alloys) for the needs of aerospace industry have found their application [1–3]. xBeam 3D Metal Printer, developed at PJSC «NVO «Chervona Hvilya» is a characteristic example of realization of such a technology in Ukraine [4]. This technology envisages a layer-by-layer formation of typical products by EBS under deep vacuum that allows effectively focusing the electron beam, and avoiding metal contamination by interstitial impurities in the case of its high affinity to oxygen and/or nitrogen. The substrate of the formed product is placed into the power fixture on a mobile platform, which moves relative to a stationary heat source with set speed V_s (Figure 1). The heat source is a component of a complex system of beam focusing and filler wire feeding. The electron beam is focused so that it had the form of a sharp cone that converges maximum close to the surface of the formed part. This allows realization of an effective and rather uniform melting of the filler wire without its significant overheating, as well as ensures concurrent heating of the deposition area for activation of the solid metal surface before its contact with the liquid filler material.

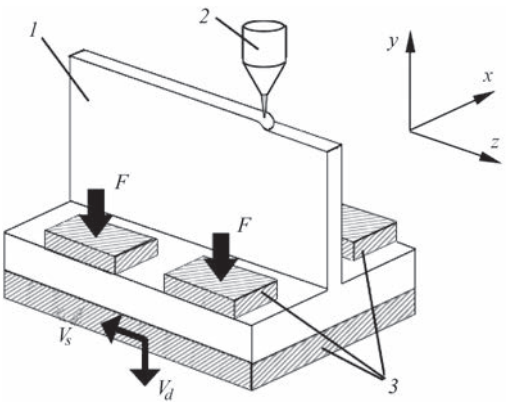

Figure 1. Scheme of formation of the web of a T-beam structure using xBeam 3D Metal Printer technology: *1* — product being formed; *2* — heat source; 3 — technological fixture

In order to manufacture products of guaranteed quality, it is necessary to optimize the technological parameters of the respective production processes.

[*]By materials of the paper presented at the International Conference «Beam Technologies in Welding and Materials Processing», September 9–13, 2019, Odessa (O.V. Makhnenko, N.S. Ananchenko, D.V. Kovalchuk also participated in the work).

O.S. Milenin — http://orcid.org/0000-0002-9465-7710, S.M. Kandala — http://orcid.org/0000-0002-2036-0498/

In particular, it concerns ensuring fusion of the successive deposited layers, homonegeity of the metal structure, low level of residual strains and stresses. As conducting a broad range of experimental studies is associated with considerable economic expenses, it is rational to apply the mathematical and computer modeling of the processes determining the final quality of products.

As part of this study, a complex of approaches were developed for numerical prediction of the kinetics of temperature fields, phase and structural states, mechanical stresses and strains at layer-by-layer formation of typical beam structures of different size by xBeam 3D Metal Printer technology, in order to study the features of the impact of the technological parameters on the current and final state of the products.

Development of the mathematical model of the kinetics of temperature and stress-strain state of typical structural elements at layer-by-layer formation of the sample. Prediction of temperature field development is the first stage of numerical study of the kinetics of the product state during layer-by-layer formation. In its turn, nonuniform heating, change of the structural composition, as well as temperature dependencies of metal properties determine the spatial distribution of stresses and strains in the structure. Temperature distribution in time and space is determined by the processes of conductive propagation, for which the connection between moment of time t and temperature field $T = T(x, y, z)$ is described by a three-dimensional equation of heat conductivity [5]:

$$c\rho(x, y, z, T)\frac{\partial T(x, y, z)}{\partial t} = \nabla\left[\lambda(x, y, z, T)\nabla T(x, y, z)\right], \quad (1)$$

where λ, $c\rho$ are the heat conductivity and volumetric heat capacity of the structure material in this point as functions of spatial coordinates and temperature, respectively.

The heat source in the considered case is the electron beam of power q_i. It must be further noted that use of filler material means that part of the source energy is consumed in its melting, and heat application to the structure can proceed in two ways: directly from the source and by molten metal transfer onto the formed product. This can be taken into account by direct change of the structure profile, by adding sections, the temperature T_m *of* which is a little higher than liquidus temperature T_L, in order to allow for filler material overheating. Here, the value of effective heat input of the source must be reduced by the value of energy consumption for filler metal melting q_m. Thus, energy distribution in the heat spot can be described by the normal distribution law, which has the following mathematical expression:

$$q(x, z) = \eta(q_I - q_m)\exp\left[-\frac{(x - x_0)^2}{K_x} - \frac{(z - z_0)^2}{K_z}\right], \quad (2)$$

$$q_m = \int_{T_C}^{T_m} c\rho(T)v_m S_m dT + g_{ft}v_m S_m \rho(T_L),$$

where η is the efficiency of the heat source (thermal efficiency); x_0, z_0 are the coordinates of the heat source center; K_x, K_z are the coefficients of concentration of energy flow in the respective directions; ρ is the density of structure metal, as a function of temperature; v_m is the filler material feed rate; S_m is the cross-sectional area of the wire; g_{ft} is the latent heat of melting of the filler material.

Boundary conditions required for solving problem (1), depend on the nature of heat removal from the product surface. So, in the area of contact with the technological fixture, the heat removal can be described by the Newton's law, whereas on the free surface it is characterized by thermal radiation (Stefan–Boltzmann law) with additional energy input from the surface of the product, being processed, when a heat source is placed there. Thus, boundary conditions for solving the heat conductivity problem in this case have the following mathematical expression:

$$-\lambda(T)\frac{\partial T}{\partial n} = \begin{cases} \alpha_{h.t}(T - T_{en}), \text{ in the area of contact with the fixture} \\ \varepsilon\sigma_{SF}(T^4 - T_{en}^4) - q, \text{ on free surfaces} \end{cases}, \quad (3)$$

where n is the normal to the surface; $\alpha_{h.t}$ is the heat transfer coefficient; T_{en} is the ambient temperature; ε is the degree of material blackness; σ_{SF} is the Stephan–Boltzmann constant; q is the energy flow of electron beam heating.

Proceeding from the results of prediction of the temperature field kinetics at layer-by-layer formation of typical products from VT6 titanium alloy, it is possible to predict the metal grain size and its certain properties in different parts of the structure, depending on the technological parameters of the process. It is known that refinement of the structural components of typical titanium-based alloys occurs with increase of the cooling rate at solidification. Figure 2 shows the dependence of grain size for VT6 alloy on the cooling rate [6], which can be approximated by the following equation:

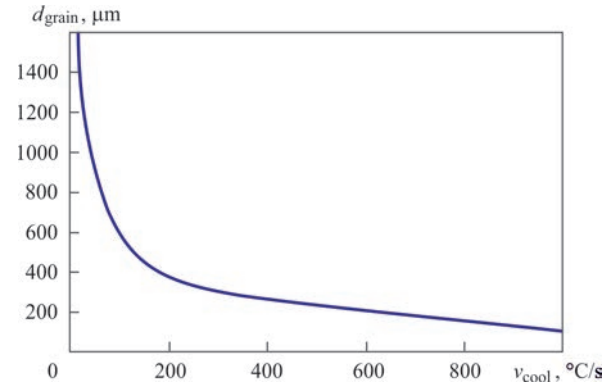

Figure 2. Dependence of grain size of VT6 titanium alloy on cooling rate [6]

$$d_{\text{grain}} = \begin{cases} 8220 v_{\text{cool}}^{-0.58} \text{ μm, at } v_{\text{cool}} \geq 6 \text{ °C/s} \\ 2500 \text{ μm, at } v_{\text{cool}} < 6 \text{ °C/s} \end{cases}, \quad (4)$$

where d_{grain} is the characteristic size of the metal grain; v_{cool} is the cooling rate.

In addition, the actual mechanical characteristics of VT6 alloy depend on the cooling rate at phase transformation, that determines the residual percent ratio of α-phase in (α+β)-alloy. Figure 3 gives the diagrams of microstructural transformations of VT6 alloy at

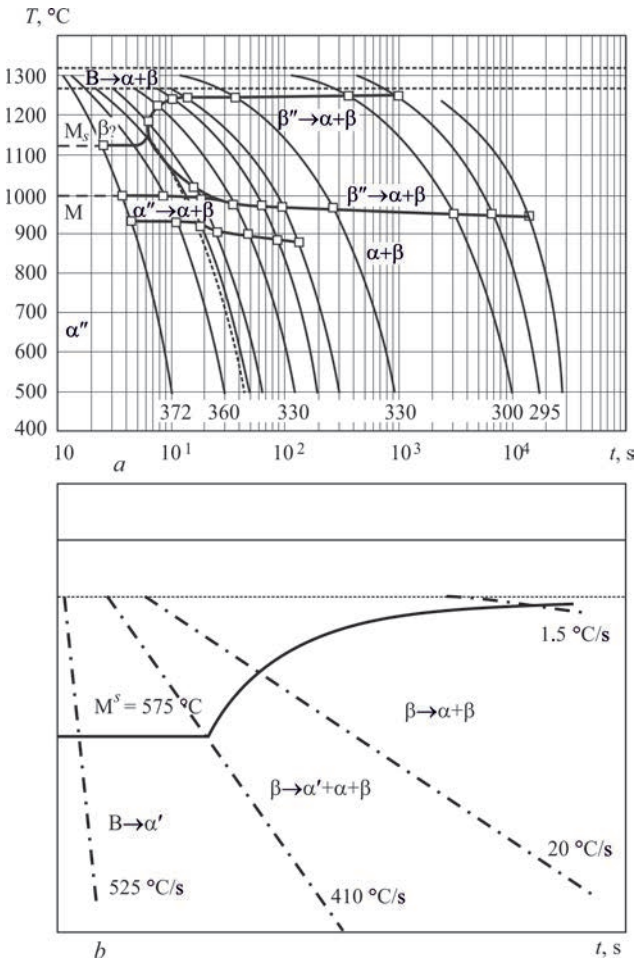

Figure 3. Diagrams of microstructural transformations of VT6 alloy at cooling: *a* — [7]; *b* — [8]

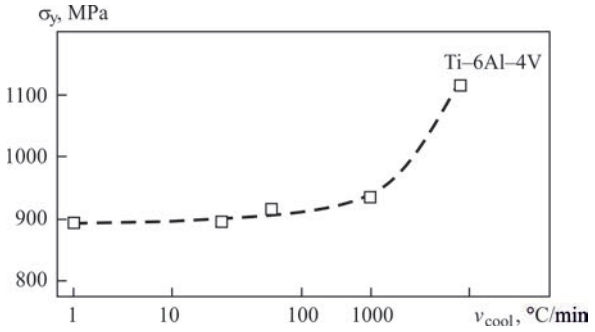

Figure 4. Dependence of yield limit of VT6 alloy on cooling rate [9]

cooling [7, 8], the cooling rate is determined in the range of β to (α+β) microstructural transformations, which proceed in the range from 1000 to 670 °C. It should be noted that owing to low heat input and high speeds of heat source movement, layer-by-layer EBS is characterized by a rather high intensity of deposited material cooling that promotes formation of a martensitic microstructure containing α′-phase. As one can see from Figure 4 [9], and at increase of the cooling rate and, accordingly, at reduction of the grain size the yield limit of VT6 alloy increases. Data in Figure 5 [8], which were derived on additive technology of layer-by-layer formation of samples by EBS method show that increase of the relative content of α′-phase $V_{\alpha'}$ causes a slight lowering of the yield limit of VT6 alloy, and relative elongation δ here decreases fairly moderately (Figure 5, *b*). These dependencies can be approximated by the following equations:

$$\begin{aligned} \sigma_y &= 995 - 0.107 v_{\text{cool}} - 18 V_{\alpha'}, \text{ MPa}, \\ \delta &= -9 V_{\alpha'} + 10.9, \%. \end{aligned} \quad (5)$$

Mathematical consideration of the united problem of temperature field kinetics and SSS development is based on finite element description with application of eight-node finite elements (FE). Within FE volume the distributions of temperatures, stresses and strains are taken to be uniform. Increment of strain tensor can be presented as superposition of the following components [10]:

$$d\varepsilon_{ij} = d\varepsilon_{ij}^e + d\varepsilon_{ij}^p + \delta_{ij} d\varepsilon_t, (i, j = x, y, z), \quad (6)$$

where $d\varepsilon_{ij}^e$, $d\varepsilon_{ij}^p$, δ_{ij}, $d\varepsilon_t$ are the components of increment of the tensor of strains, due to elastic mechanism of deformation, instantaneous plasticity strains, and temperature expansion, respectively; δ_{ij} is the Kronecker symbol.

Tensors of mechanical stresses σ_{ij} and elastic strains $d\varepsilon_{ij}^e$ are connected to each other by a generalized Hooke's law, i.e.

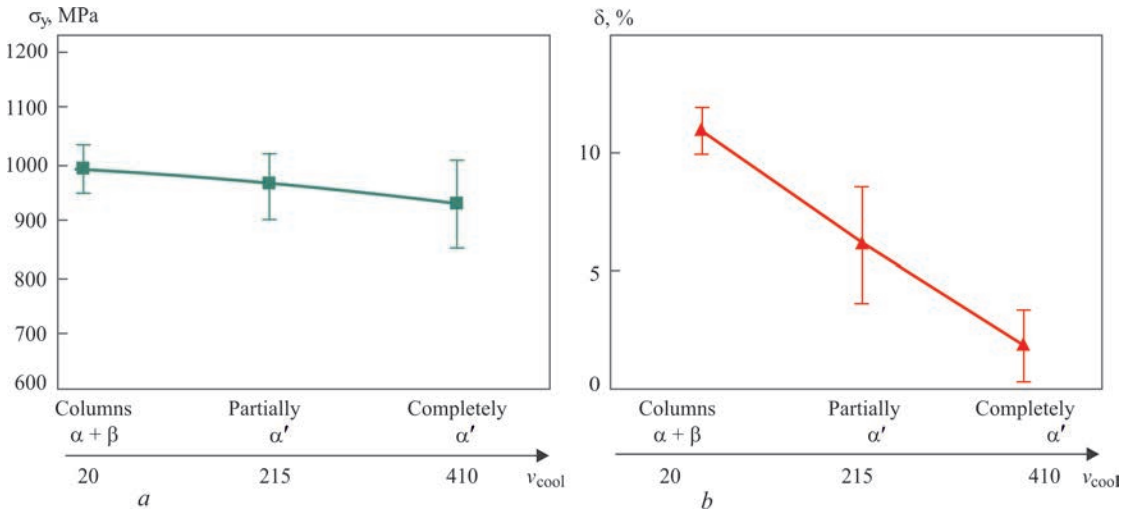

Figure 5. Dependence of yield limit (*a*) and relative elongation (*b*) of VT6 alloy on cooling rate and quantity of α′-phase [8]

$$\varepsilon_{ij}^{e} = \frac{\sigma_{ij} - \delta_{ij}\sigma}{2G} + \delta_{ij}(K\sigma + \varphi), \qquad (7)$$

where σ is the average value of the normal components of stress tensor σ_{ij}, i.e. $\sigma = \left(\sigma_{xx} + \sigma_{yy} + \sigma_{zz}\right)/3$; $K = (1-2\nu)/E$ is the volumetric compression modulus; G is the shear modulus; E is the Young's modulus; υ is the Poisson's ratio; φ are the volumetric strains.

Increment of instantaneous plasticity strain $d\varepsilon_{ij}^{p}$ in a specific FE was calculated using a linear dependence of scalar function Λ and deviator component of the stress tensor, namely:

$$d\varepsilon_{ij}^{p} = d\Lambda(\sigma_{ij} - \delta_{ij}\sigma). \qquad (8)$$

Specific value of function Λ depends on the stressed state in the considered area of the structure, as well as on the shape of the surface of material plastic flow Φ, which is characterized by stresses σ_S:

$$\begin{aligned} &d\Lambda = 0, \text{ if } \sigma_i < \sigma_s, \\ &d\Lambda > 0, \text{ if } \sigma_i = \sigma_s, \\ &\text{state } \sigma_i > \sigma_s \text{ is inadmissible,} \end{aligned} \qquad (9)$$

where σ_i is the stress intensity.

Proceeding from the above-said, the increments of strain tensor can be presented as superposition of increment of the respective components:

$$\begin{aligned} \Delta\varepsilon_{ij} = \Psi\left(\sigma_{ij} - \delta_{ij}\sigma\right) + \delta_{ij}\left(K\sigma + \Delta\varepsilon_{t}\right) - \\ - \frac{1}{2G}\left(\sigma_{ij} - \delta_{ij}\sigma\right)^{*} - \left(K\sigma\right)^{*}, \end{aligned} \qquad (10)$$

where symbol «*» refers the respective variable to the previous trace step; ψ is the function of material state, which determines the plastic flow condition according to Mises criterion:

$$\begin{aligned} &\psi = \frac{1}{2G}, \text{ if } \sigma_i < \sigma_s = \sigma_y, \\ &\psi > \frac{1}{2G}, \text{ if } \sigma_i = \sigma_s, \text{ state } \sigma_i > \sigma_s \text{ is inadmissible.} \end{aligned} \qquad (11)$$

Function ψ is determined by iteration at each step of numerical tracking within the boundary problem of nonstationary thermoplasticity that allows solving the nonlinearity by plastic flow of the material. Proceeding from the specific value of function ψ from (11), the strain filed is defined at each stage of loading, taking into account dependence $\sigma_s(T, \varepsilon_p)$:

$$\Delta\varepsilon_{ij} = \left(\xi - \frac{1}{2G}\right)\left(\sigma_{ij} - \delta_{ij}\sigma\right). \qquad (12)$$

Here, at each stage of iteration by ψ, stress σ_{ij} is calculated by the following algorithm (repeated indices are summed up):

$$\sigma_{ij} = \frac{1}{\psi}\left(\Delta\varepsilon_{ij} + \delta_{ij}\frac{\psi - K}{K}\Delta\varepsilon\right) + J_{ij}, \qquad (13)$$

where

$$\Delta\varepsilon = \frac{\Delta\varepsilon_{ii}}{3},$$

$$J_{ij} = \frac{1}{\psi}\left[\left(b_{ij} - \delta_{ij}b\right) + \delta_{ij}\left(K\sigma^{*} - \frac{\Delta\varepsilon_{t}}{K}\right)\right], \qquad (14)$$

$$b_{ij} = \left(\frac{\sigma_{ij}}{2G}\right)^{*} + \delta_{ij}\left[\sigma_{m}^{*}\left(K - \frac{1}{2G}\right)^{*} - \Delta\varphi\right], b = \frac{b_{ij}}{3}.$$

Stress tensor components satisfy the statics equations for internal FE and boundary conditions for the surface ones. In their turn, the components of displacement vector $\Delta U_i = (\Delta U, \Delta V, \Delta W)$ satisfy the respective conditions on the boundary. The solved system of equations in variables of the vector of dis-

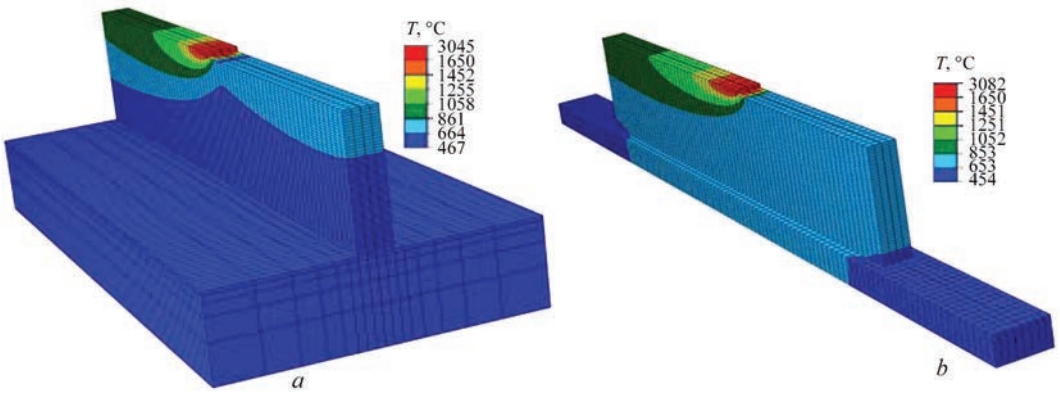

Figure 6. Comparative distribution of temperatures in a T-shaped sample with large (*a*) and small (*b*) substrates during layer-by-layer formation of the part

placement increments in FE nodes at each trace step and iteration by ψ is determined by minimizing the following functional (Lagrange variational principle):

$$Э_1 = -\frac{1}{2}\sum_V \left(\sigma_{ij} + J_{ij}\right)\Delta\varepsilon_{ij} V_{m,n,r} + \sum_{S_P} P_i \Delta U_i \Delta S_P^{m,n,r}, \quad (15)$$

where $\sum_V$ is the sum operator for internal FE; $\sum_{S_P}$ is the sum operator for surface FE, on which the components of force vector P_i are assigned, i.e. the following system of equations yields a solution in the components of the vector of displacement increments at each trace step and iterations by ψ for a specific FE:

$$\frac{\partial E_1}{\partial \Delta U_{m,n,r}} = 0, \quad \frac{\partial E_1}{\partial \Delta V_{m,n,r}} = 0, \quad \frac{\partial E_1}{\partial \Delta W_{m,n,r}} = 0. \quad (16)$$

Results of modeling the temperature fields at layer-by layer formation of the tee sample and prediction of the material structure and mechanical properties. Features of temperature field kinetics were studied on the typical example of layer-by-layer formation of a T-shaped beam product. The following process parameters are recommended: filler material – 1.6 mm titanium rod, electron beam power of 4.5 kW, filler wire feed rate of 14 mm/s, substrate movement speed of 14 mm/s. In order to determine the impact of geometrical features of the product, EBS on substrates of different thickness was considered, namely on massive substrate of 8×30×70 mm size; and on small one of 3×6×110 mm size. Results of solving the nonstationary heat conductivity problem showed that the kinetics of the temperature field at layer-by-layer formation of the tee sample on a massive substrate is of essentially 3D nature whereas in the case of a small substrate, sample heating by volume is more uniform (see Figure 6) that is attributable to the effect of heat accumulation.

As shown by analysis of thermal cycles (Figure 7), in the range of microstructural transformations from 1000 to 670 °C, the material is heated and cooled 3 times: first during deposition of the layer, then during deposition of the next two layers. The last cooling cycle in the above-mentioned temperature range determines the residual microstructure and grain size. Maximum heating temperature in the considered region from deposition of the next third and more distant layers is below the temperature of 1000 °C, so that no microstructural transformations or considerable change of grain size occur. Moreover, this process is characterized by rather high cooling rates (160–660 °C/s), so that in keeping with the diagrams of microstructural transformations of VT6 alloy (see Figure 2) the deposited metal of tee sample is predicted to have a martensitic microstructure, containing α′-phase. By the data of calculations in the material of the first layer, where the highest cooling rate was achieved, owing to the presence of a massive cold substrate, 180 μm grain forms, and in the points of formation of 5 and 20 layers, where material is deposited on the already heated sample, grain size is much larger and reaches 300–450 μm.

These results comply with the available experimental data [4] on the microstructure of a sample of VT6 titanium alloy, produced by xBeam 3D Metal Printer technology of layer-by-layer formation: grain size in the upper layers of the sample is equal to approximately 300–450 μm, and in the layers near the sample base it is 150–250 μm (Figure 8). Thus, pre-

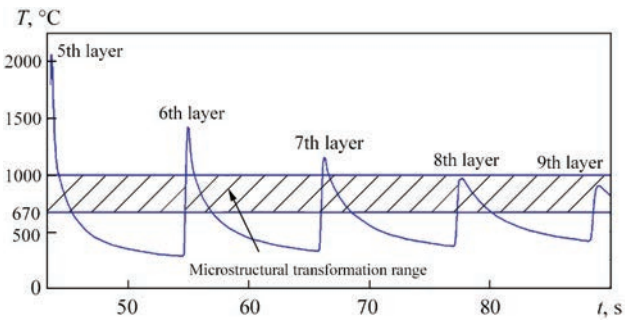

Figure 7. Characteristic thermocycle in T-shaped sample material (5th layer) at multilayer formation

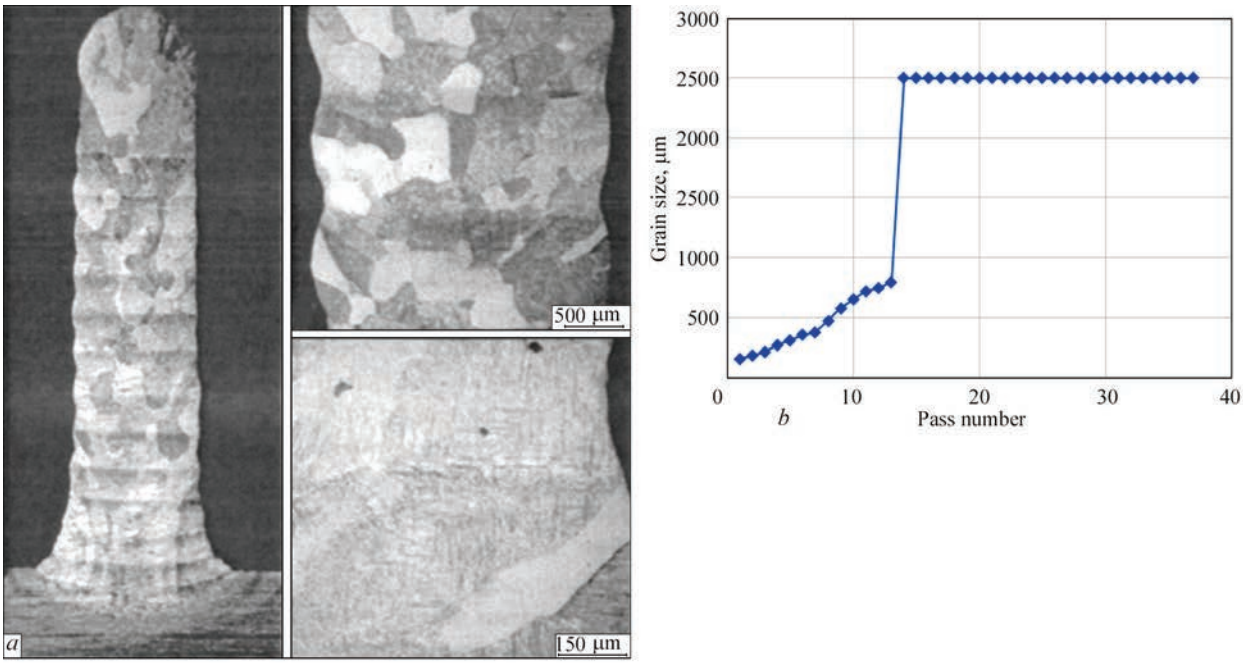

Figure 8. Macrostructure of a tee sample from VT6 titanium alloy: *a* — experimental study [11]; *b* — calculation results

diction results showed satisfactory accuracy, compared with the experiment that allows application of the developed mathematical model for prediction of the macrostructure and mechanical properties of the metal of structures produced by such technologies.

As was shown by the authors in previous works, one of the effective ways to optimize the temperature fields at layer-by-layer formation of typical beam structures is application of delay time Δt of deposition of each of the beads, variable by product height

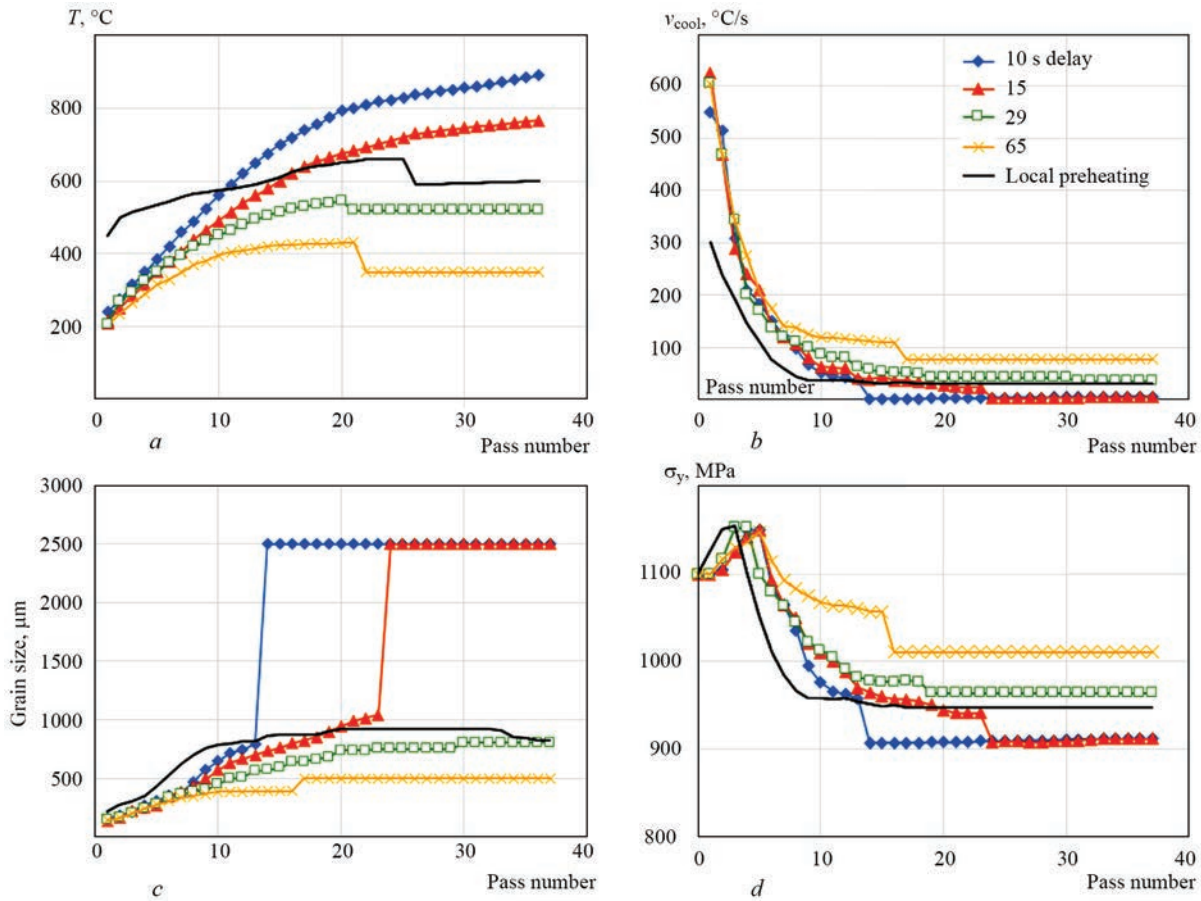

Figure 9. Dependence of temperature in the point before deposition of the next layer (*a*), cooling rate (*b*), grain size (*c*) and material yield limit (*d*) on pass number for different delay times between the passes

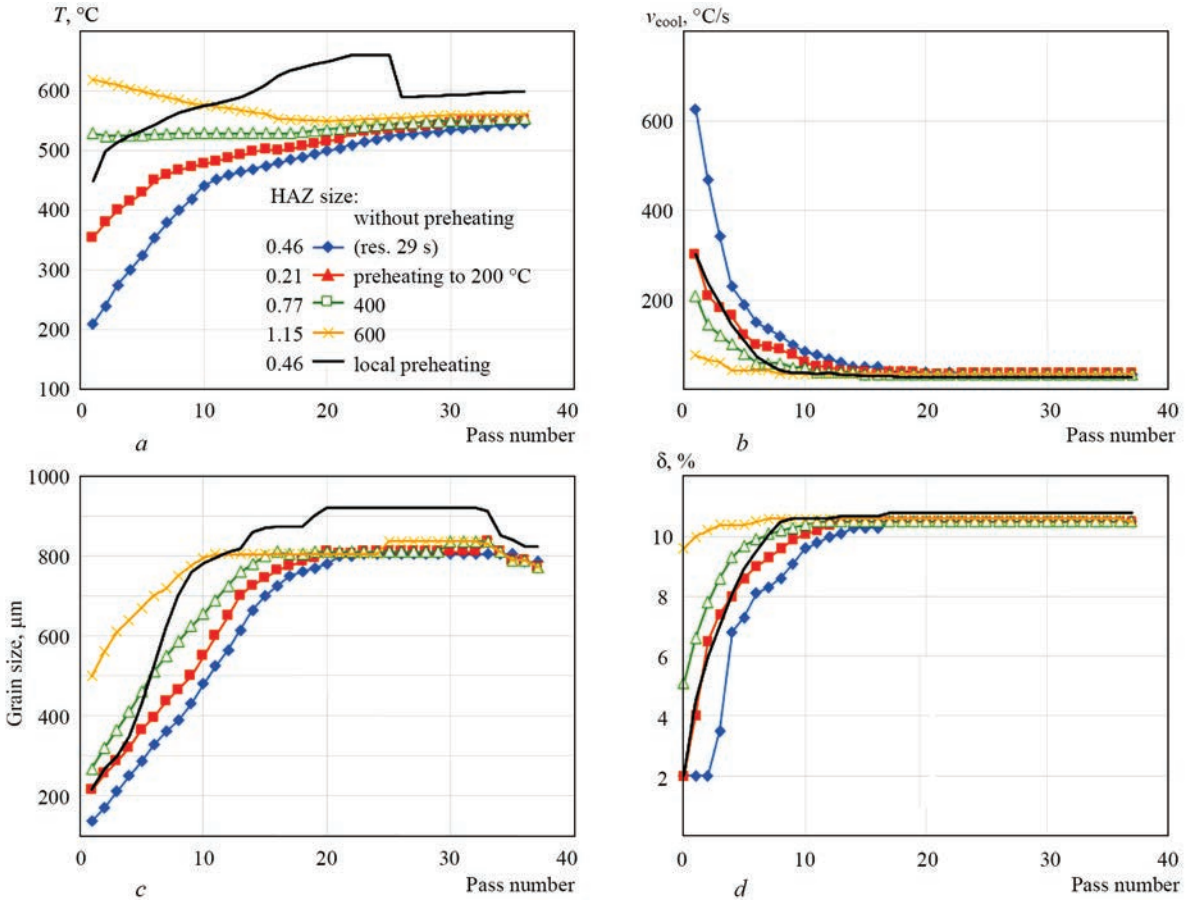

Figure 10. Dependence of temperature in a point before deposition of the next layer (*a*), cooling rate (*b*), grain size (*c*) and relative elongation (*d*) on pass number for different preheating of the substrate

[11]. This allows ensuring the natural dissipation of excess heat, which accumulates as the product layers are deposited, and avoid its overheating without the need for variation of the power (speed) of the heat source. This technological parameter essentially affects the cooling rate, grain size, and, consequently, the product material yield limit (Figure 9, *a*–*c*). One can see from the given data that the best strength characteristics and more uniform material structure were determined in the sample, made with longer time Δt, whereas the insufficient time between bead deposition Δt = 10 s and 15 s results in insufficient strength characteristics of metal in the upper layers, and grain nonuniformity by height. On the other hand, too long time between the passes (65 s) leads to formation of an excess of α′-phase, and reduction of material plasticity. Substrate preheating allows obtaining a more uniform structure in the lower layers, and essentially improves the material plasticity (Figure 10, *a*–*c*). For the time between bead deposition Δt = 10 s and 15 s the grain size increases significantly, starting from the number of the bead, on which the interpass temperature exceeds 670 °C: then the grain is finally formed after complete cooling of the sample, and the cooling rate here is low. When the time between beads deposition is Δt = 29 s, the interpass temperature does not exceed 670 °C, so that the produced grain is more uniform.

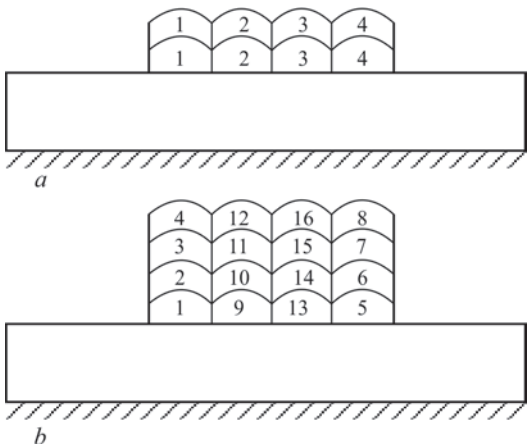

Figure 11. Characteristic sequences of bead deposition at formation of T-shaped beam structure: *a* — layer-by-layer deposition (scheme A); *b* — column deposition (scheme B)

Characteristic features of residual stress-strain state at layer-by-layer formation of thick-walled T-shaped products by xBeam 3D Metal Printer technology. In the previous works the authors studied the features of the kinetics of stress-strain state (SSS) during layer-by-layer formation of beam, cylindrical and spherical structural elements, using xBeam 3D Metal Printer technology [11]. In particular, it was em-

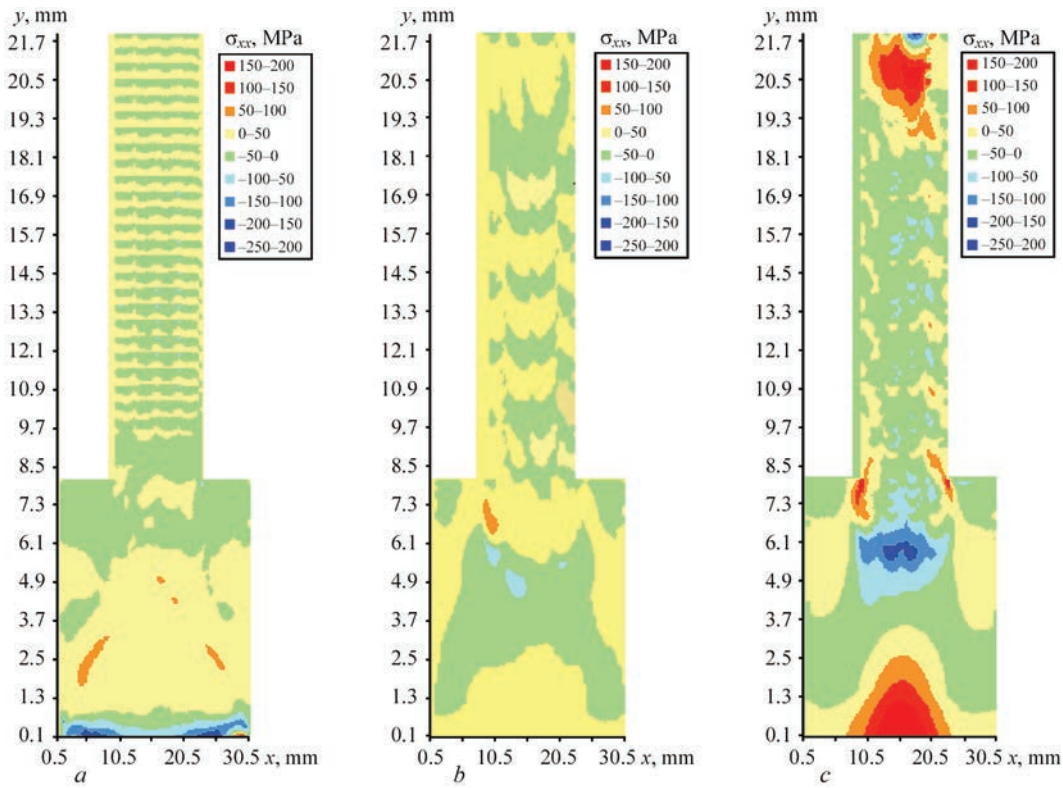

Figure 12. Distribution of residual stresses, σ_{xx} (MPa) in the cross-section of a T-shaped product: *a* — scheme A with optimization; *b* — scheme B with optimization; *c* — scheme B without optimization (see Figure 11)

phasized that one of the advantages of this technology is the possibility of deposition of rather narrow beads of liquid metal and production of thin-walled structural elements (with 2–3 mm wall thickness) with small geometrical tolerances. However, xBeam 3D Metal Printer applicability is not limited to just thin-walled products: various sequences of forming bead deposition can be used, if it is necessary to manufacture

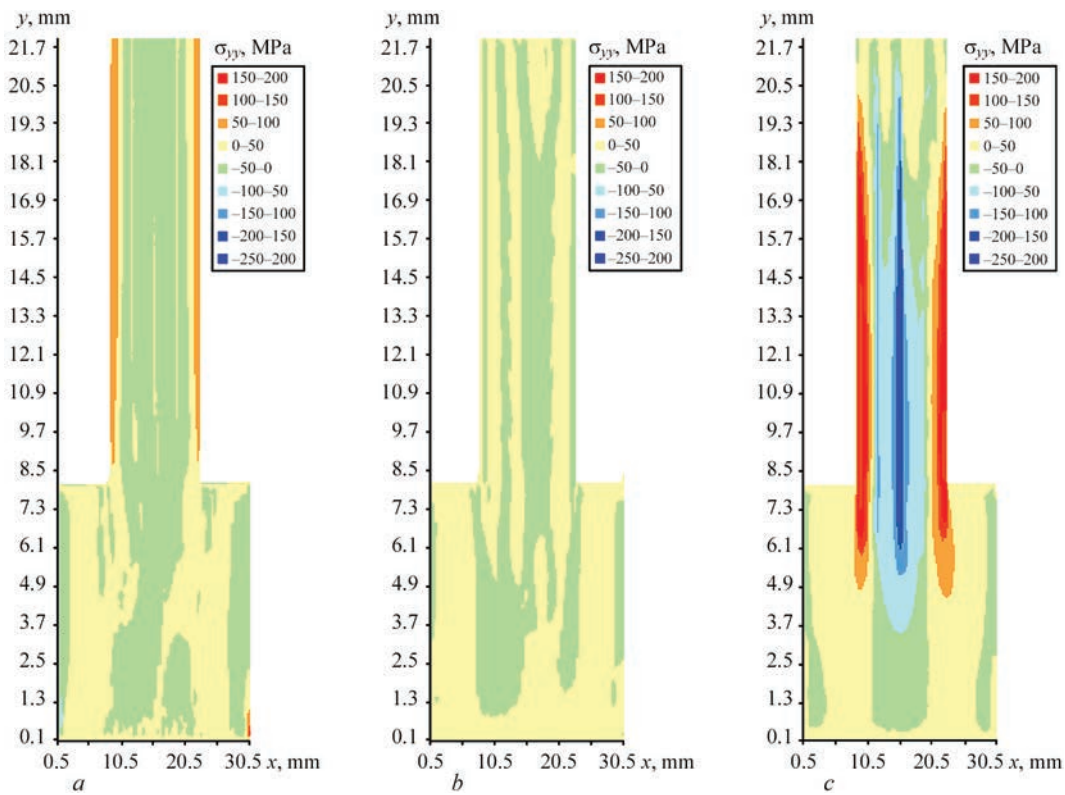

Figure 13. Distribution of residual stresses σ_{yy} (MPa) in the cross-section of a T-shaped product: *a* — scheme A with optimization; *b* — scheme B with optimization; *c* — scheme B without optimization (see Figure 11)

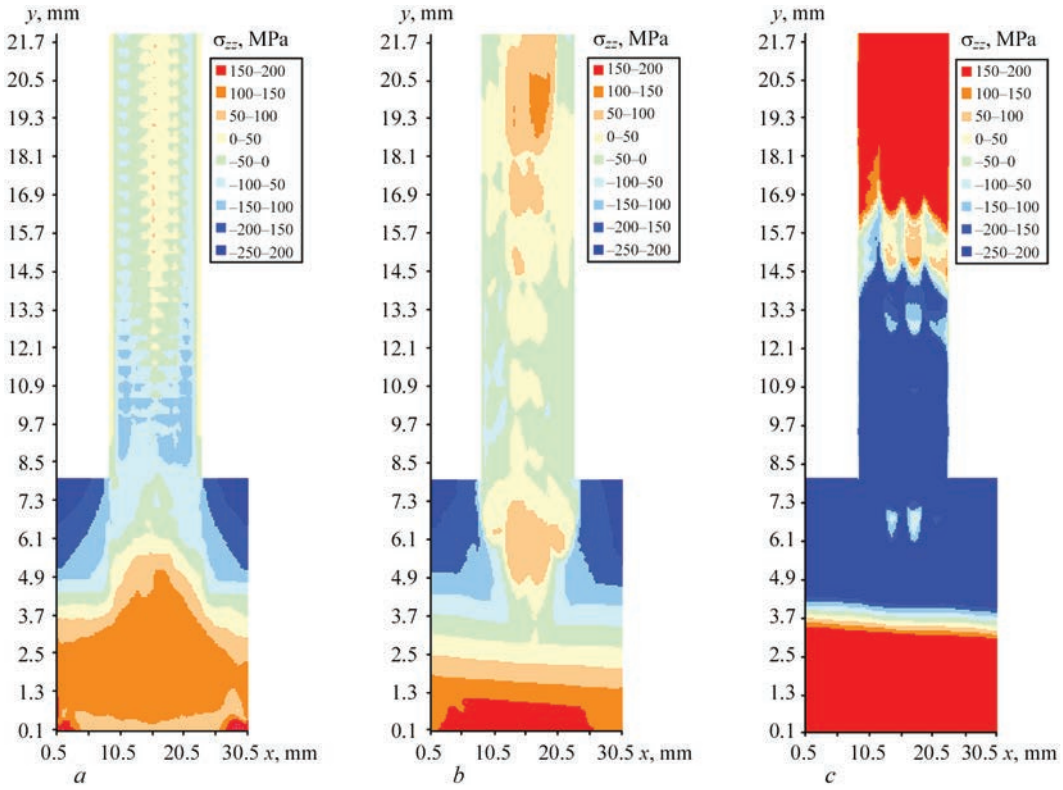

Figure 14. Distribution of residual stresses σ_{zz} (MPa) in the cross-section of a T-shaped product: *a* — scheme A with optimization; *b* — scheme B with optimization; *c* — scheme B without optimization (see Figure 11)

thick-walled parts. These sequences allow producing structures with different wall thickness without any essential change of the respective technological parameters. However, such a process certainly requires optimization, in particular, from the viewpoint of rational selection of the time of the start of each bead formation (delay time Δt) and formation of favourable residual SSS.

Within the scope of this work, the features of residual SSS depending on the technological conditions of production were studied in the case of a thick-walled T-shaped beam. Considered were two typical sequences of deposition of a tee wall of 12.8 mm thickness, which consists of four parallel beads 3.2 mm thick and 0.8 mm high (Figure 11). Structure material was VT6 titanium alloy. The principal difference between these schemes consists in that for sequence A the web is formed by successive horizontal layers, whereas for sequence B vertical columns are the forming elements.

Figures 12–14 show the results of prediction of the residual stress fields in the cross-section of a thick-walled beam for sequences A and B, taking into account optimization of the temperature fields by selection of optimum delay time Δt, as well as deposition by sequence B without such optimization. As one can see from the given results, the temperature field optimization allows achieving structure heating sufficiently uniform by thickness, despite the different sequence of bead deposition. Thus, the conditions for uniform cooling of the product, and, accordingly, low level of residual stresses, are in place. A natural stress raiser in such a case is the region of transition of the tee section flange into the web, where the uniform cooling conditions are not fulfilled for the reason of massiveness of the substrate (tee section flange). If the conditions of the temperature field optimization are not fulfilled, and the structure is nonuniformly heated, it leads to formation of high stresses, particularly, in the longitudinal direction (see Figure 14, *c*). Therefore, a rational selection of the delay time between the deposited beads is important not only in terms of guaranteeing the conditions, favourable for sound formation of the product, but also for lowering the residual stresses, that is required for high performance of the produced structural elements.

Conclusions

1. A complex of mathematical models was developed for numerical prediction of the temperature field kinetics, phase and structural states, mechanical stresses ad strains at layer-by-layer formation of typical beam structures from VT6 titanium alloy, using xBeam 3D Metal Printer technology. Comparison with the data of experimental studies showed the satisfactory accuracy of the obtained calculation results of prediction of the macrostructure and mechanical properties of the structure metal.

2. The impact of substrate dimensions on temperature field kinetics during layer-by-layer deposition of a web of a tee section was studied. It is shown that in case of a massive substrate 8 mm thick temperature distribution is of an essentially 3D nature, whereas for the case of a small substrate of 3 mm thickness, more uniform heating of the sample by volume is in place, that is attributable to heat accumulation effect.

3. It is shown that better strength characteristics and more uniform structure of the material of the part, produced by layer-by-layer formation, can be achieved at maximum increase of the delay time between beads deposition, whereas insufficient time results in lower strength characteristics of metal in the upper layers, and nonuniformity of the grain by height. However, increase of time between the passes may lead to formation of an excess of α′-phase, and lowering of material plasticity. An effective means for producing a more uniform structure and improvement of material plasticity is preheating of the plate before the beginning of structure fabrication.

4. A characteristic example of layer-by-layer formation of T-shaped beam structure was used to study the regularities of the residual stressed state in fabrication of thin-walled structures. It is proved that optimization of delay time at deposition of each of the beads is an important factor, allowing achievement of a low level of residual stresses. Here, conditions are in place for uniform cooling of the structure (except for the region of transition of the tee flange into the web) and an essential lowering of residual stresses. Violation of the optimal thermal mode can lead to an essential increase of residual stresses (particularly, longitudinal), creating a negative effect on such a structure performance.

1. Edwards, P. et al. (2013). Electron beam additive manufacturing of titanium components: Properties and performance. *J. of Manufacturing Sci. and Eng.*, 135(**6**). DOI: 061016/1-061016/7.
2. Juechter, V., Franke, M.M., Merenda, T. et al. (2018) Additive manufacturing of Ti–45Al–4Nb–C by selective electron beam melting for automotive applications. *Additive Manufacturing*, **22**, 118–126. DOI: 10.1016/j.addma.2018.05.008.
3. Dutta, B., Froes, F.H. (2016) *Additive manufacturing of titanium alloys: State of the art, challenges and opportunities*. Oxford, Butterworth-Heinemann. DOI: 10.1016/C2015-0-02470-4.
4. Kovalchuk, D.V., Melnik, V.I., Melnik, I.V. (2017) New possibilities of additive manufacturing with xBeam 3D Metal Printing technology. In: *Proc. of 8th Int. Conf. on Beam Technologies in Welding and Processing of Materials*. Kyiv, 45–52.
5. Makhnenko, V.I. (2006) *Safe service life of welded joints and assemblies of modern structures*. Kyiv, Naukova Dumka [in Russian].
6. Polkin, I.S. (2006) Improvement of properties of metallic materials due to application of new technological processes. In: *Advanced technologies of light and special alloys*. Moscow, Fizmatlit, 66–73 [in Russian].
7. Sieniawski, J., Ziaja, W., Kubiak, K. (2013) Microstructure and mechanical properties of high strength two-phase titanium alloys. *Titanium Alloys*, 69–79.
8. Liu, S., Shin, Y.C. (2019) Additive manufacturing of Ti6Al4V alloy: A review. *Materials and design*, **164**, 1–23.
9. Patil, S., Kekade, S., Phapale, K. (2016) Effect of α and β phase volume fraction on machining characteristics of titanium alloy Ti6Al4V. In: Proc. of *16th Machining Innovations Conf. for Aerospace Industry*, 65.
10. Velikoivanenko, E.A., Milenin, A.S., Popov, A.V. et al. (2019) Methods of numerical forecasting of the working performance of welded structures on computers of hybrid architecture. *Cybernetics and Systems Analysis*, 55(**1**), 117–127. DOI: 10.1007/s10559-019-00117-8.
11. Makhnenko, O.V., Milenin, A.S., Velikoivanenko, E.A. et al. (2017) Modelling of temperature fields and stress-strain state of small 3D sample in its layer-by-layer forming. *The Paton Welding J.*, **3**, 7–14. DOI: 10.15407/tpwj2017.03.02.

Received 21.11.2019